

---

## **Chapter 2**

### ***Novolac type phenolic resin- based networks***

### ***For the removal of azo dyes from aqueous solutions***

---

## **2.1 Introduction**

Azo dyes are the largest and most versatile class of organic dye-stuffs. They are found in the effluent water of several industries such as textile, leather, paper, pharmaceutical, plastic, and food. Most of these dyes and their degradation products are known to be toxic, carcinogenic, mutagenic and teratogenic causing damage to both human health and ecosystem. Therefore, it is extremely important to get rid of these azo-dye pollutants from waste water before discharge into water streams. Among different removal approaches, absorption is regarded as an easy, effective and economic process in producing high-quality effluent without the formation of harmful substances. Review in this direction has already been made in previous introductory chapter. Especially, polymeric sorbents, which can effectively extract organic pollutants from waste streams, are quite attractive, because of their advantageous features as discussed in *Chapter-1*. However, the literature survey in *Chapter-1* indicated that the examples of azo-dye removing polymeric sorbents are limited. Furthermore, phenolic resins are a class of easily achievable, three dimensional synthetic materials as discussed briefly in *Chapter-1*. However, despite their promising features, they have been explored very little in the design of polymeric adsorbents for waste water treatments to remove dye pollutants. Meanwhile, ligation chemistry of low

molecular weight amines, such as ethylene diamine and diethylene triamine is a matter of great interest due to their basicity and nonhydrolyzability. Accordingly, the design and synthesise of novolac phenolic resin-baesd polymeric network type sorbents incorporating the structural features of both novolac and amines is a worthwhile and challenging undertaking. This chapter is based upon our publications<sup>2.1-2.3</sup> (included in the Appendix) focusing on the development of novolac-based networks to remove azo-dyes from water.

## 2.2 Objective

The attention of this chapter is drawn to the design and synthesis of novolac type phenolic resin-based network polymers (2.3 and 2.4) as illustrated in Figure 2.1 and their potential application in adsorptive removal of selected azo dye molecules from aqueous medium..

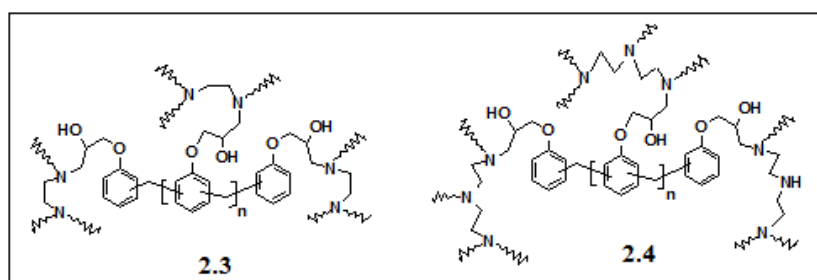


**Figure 2.1** The structures of target novolac-based polymeric networks

## **2.3 Experimental Section**

### **2.3.1 Materials and Measurements**

Chemicals were purchased and used without purification. NMR spectra were recorded on Bruker NMR spectrometer. FTIR spectra were recorded on Perkin Elmer spectrophotometer using KBr discs. Molecular weights and molecular weight distribution of **2.2** were determined by Waters gel permeation chromatography instrument in THF as an eluent, calibrated by polystyrene standards at 30<sup>0</sup>C. Elemental analyses were performed on 2400 Series II CHN analyser (Perkin Elmer) using helium as driving gas and oxygen as combustion gas. TGA/DTG analyses were conducted with Perkin Elmer Diamond TG/DTA instrument under nitrogen atmosphere. Surface morphology of polymer network was examined by a scanning electron microscope (JEOL JSM-5800). UV-vis spectra were recorded on ShimadzuUV-1800 spectrophotometer. Laser diffraction particle size analysis was performed on HELOS (H1004) & SUCCELL analyzer, using deionized water as the dispersant. After few seconds of ultrasonication the dispersions of the network powder were introduced into the dispersion unit device of the laser particle analyzer for measurements. A pH meter ( Tosniwall, CL 46 ) was employed for the pH measurements. Brunauer-Emmette-Teller (BET) surface area analysis<sup>2,20</sup> was carried out using ASAP 2020 Micrometrics instrument under nitrogen environment. Degasification of the network sample was done at 350 °C for 6 h before analysis.

### **2.3.2 Synthesis of novolac resin 2.1**

The synthesis was performed utilizing phenol and formaldehyde in the ratio of 1.2 : 1. In the reaction, a stoichiometric amount of formaldehyde and phenol were taken in water and refluxed for 30min in the presence of oxalic acid catalyst (1.2 mmol). Then another 1.2 mmol oxalic acid was added and refluxing was continued for 1h. An oily layer appeared, was separated and dried over anh. Na<sub>2</sub>SO<sub>4</sub> to yield the product. FT- IR (KBr):  $\nu_{\max}$  = 3442, 2919, 2846, 1604, 1501, 1379, 1256, 1095, 1005 (w), cm<sup>-1</sup>; <sup>1</sup>H NMR (DMSO-d<sub>6</sub>, 400MHz)  $\delta$ : 9.31-9.11 (bm, Ar-OH, H-bonded), 7.16 (t, J= 12Hz, ArH), 6.98-6.88 (m, ArH), 6.76 (m, ArH), 6.66 (m, ArH), 3.79-3.64 (m, Ar-CH<sub>2</sub>-).

### **2.3.3 Synthesis of novolac epoxy resin 2.2**

A mixture of **2.1** (3.5g), 1-Chloro-2,3-epoxypropane (47.2g, 0.51mol), NaOH (0.8g) in 5ml water was stirred in a water bath for 30 min. Then another 0.7g NaOH was added and heating was continued for 40 min. The light violet color gradually turned to yellow. The organic layer was separated and excess 1-chloro-2,3-epoxypropane was removed in vacuo. Then the organic phased was washed with water repeatedly. The residual water in organic phase was

removed under reduced pressure to yield the product. FT- IR (KBr):  $\nu_{\max}$  = 3431, 2936, 1640, 1387, 1008, 904  $\text{cm}^{-1}$ ;  $^1\text{H}$  NMR (DMSO- $d_6$ , 400MHz)  $\delta$ : 7.29 (t, J= 10Hz, ArH), 7.12-7.09 (m, ArH), 6.96 (d, J=8Hz, ArH), 6.86 (bm, ArH), 3.98-3.63 (bm, ArOCH<sub>2</sub>-, Ar-CH<sub>2</sub>-, epoxide proton), 3.57-3.51 (m, Ar-CH<sub>2</sub>-, epoxide protons), 3.24 (bm, epoxide protons), 2.86-2.83 (m, epoxide protons), 2.70 (s, epoxide protons);  $^{13}\text{C}$  NMR (CDCl<sub>3</sub>, 125 MHz)  $\delta$ : 158.33, 156.70, 155.0, 134.27, 134.10, 130.68 (unresolved), 129.43, 129.38, 127.57, 127.37, 121.24, 121.04, 114.54, 111.60, 111.31, 70.34, 69.71, 68.64, 63.48, 50.11, 45.86, 45.63, 44.85, 44.56, 44.44, 39.96, 35.64, 35.07, 30.01; GPC (using polystyrene and THF):  $M_w$  =3300, MWD 1.10.

### **2.3.4 Epoxy equivalent weight of novolac epoxy resin 2.2**

Pyridinium chloride – pyridine method was used to quantify the epoxy equivalent weight (EEW)<sup>2,21</sup> EEW of **2.2**. 1g of resin was dissolved in 25ml of standardized pyridinium chloride – pyridine solution prepared from 16 ml conc. HCl diluted with pyridine to 1 l. The solution was then heated to reflux for 3h and cooled. The difference between the amount of acid added and the amount of acid unconsumed determined by titration with standard sodium hydroxide in methanol determines the epoxy content. Epoxy content = epoxide equivalent / 100 g resin; EEW = 100/epoxy content. Epoxy equivalent weight (EEW) of **2.2** was ~515.

### **2.3.5 Synthesis of polymer network 2.3**

Novolac-based epoxy resin **2.2** (0.45 g) and ethylenediamine (0.224 g, 3.74 mmol; stoichiometric equivalent: amine N-H/epoxy group = 17 : 1) were allowed to react for 3h with stirring in a mixture of 1,4-dioxan (0.8ml) and methanol (0.4mL) at 95-100°C. The product precipitated as yellowish solid. Precipitate was filtered and purified by thoroughly washing with deionized water to obtain polymer network **2.3**. FTIR (KBr):  $\nu_{\max}$  = 3393, 2926, 2848, 1604, 1507, 1450, 1243, 1115, 1024, 805, 734  $\text{cm}^{-1}$ .  $^{13}\text{C}$  NMR (Solid state, 100 MHz)  $\delta$ : broad unresolved peaks at 154.74, 133.14, 115.83, 66.50, 56.96, 49.61, 39.47; Elemental analysis: found: C, 64.30; H, 7.18; N, 6.31%.

### **2.3.6 Synthesis of polymer network 2.4**

Novolac-based epoxy resin **2.2** (0.45 g) and diethylenetriamine (0.138g, 1.34 mmol; stoichiometric equivalent: amine N-H/epoxy group = 7.89 : 1) were allowed to react for 3h with stirring in a mixture of 1,4-dioxan (0.8ml) and methanol (0.4mL) at 95-100°C. The product precipitated as yellowish solid. Precipitate was filtered and purified by thoroughly washing with deionized water to obtain polymer network **2.4**. FTIR (KBr):  $\nu_{\max}$  = 3365, 2921, 2849, 1609, 1510, 1454, 1240, 1173, 1107, 1034, 810, 752, 691  $\text{cm}^{-1}$ ;  $^{13}\text{C}$  NMR (Solid state, 100 MHz)  $\delta$ : broad unresolved peaks at 161.87, 154.85, 130.02, 115.85, 65.44, 49.20, 39.11; Elemental analysis: found C, 63.73; H, 7.24; N, 6.97%.

### 2.3.7 Network swelling study

Fully dried disc-shaped samples prepared by an infrared (IR) pellet sampler were weighed and equilibrated in distilled water at 25 °C for 48h. The equilibrium swelling capacity or swelling ratio ( $Q$ ) was calculated as follows:  $Q = W_0 / W_d$ ; Where,  $W_0$  is the weight of water in the swollen network and  $W_d$  is the dry weight of the network. The swelling studies were repeatedly performed by thrice with 5% standard deviation.

Parameters like crosslink density ( $q$ ) and number average molecular weight between cross-links ( $M_c$ ) were calculated from the equilibrium swelling data using Flory-Rehner equation<sup>2.4,2.22,2.23</sup>.

$$M_c = - \frac{\rho_n V_s (V_n^{1/3} - V_n/2)}{\ln(1 - V_n) + V_n + \chi V_n^2}$$

Where  $\rho_n$  = density (g/cc) of network

$V_s$  = molar volume of solvent

$V_n$  = volume fraction of network, it is the water content of network sample in equilibrium swollen state.

$\chi$  = polymer-solvent interaction parameter of network/water system



$\chi$  was calculated by Flory-Huggins theory using the following equation<sup>2,24</sup>:

$$\chi = \frac{\ln(1 - V_n) + V_n}{V_n^2}$$

$V_n$  was calculated according to the following equation<sup>25</sup>:

$$V_n = \left[ 1 + \frac{\rho_n}{\rho_s} \left( \frac{W_0}{W_d} - 1 \right) \right]^{-1}$$

Where  $\rho_s$  is the density (g/cc) of solvent.  $M_c$  was calculated by using the values of  $\chi$  and  $V_n$ . The crosslink densities ( $q$ ) for the network samples were calculated<sup>2,25-2.27</sup> as follows:

$$q = \frac{1}{2M_c}$$

### **2.3.8 Porosity measurement**

Solvent replacement method was used for porosity measurement. Dried disc-shaped network samples were immersed in water at 25 °C for 48h and weighed after blotting excess of water on the surface. The porosity<sup>2,28</sup> of networks was calculated from the equation:

$$\text{Porosity} = \left( \frac{W_0}{\rho_s V} \right) \times 100$$

where  $\rho_s$  is the density of water and  $V$  is the volume of the network.

### **2.3.9 Adsorption study**

Adsorption experiments were carried out by adding pre-weighed amount of sorbents to the solutions containing azo dyes at different pH values of 2.30, 7.20 and 10.96 and shaken. The pH was adjusted to a given value with dilute NaOH or HCl solutions. After different intervals, the solutions were separated from the adsorbents, and the residual concentration of azo dye (MO/OII/OG) was determined by UV-vis spectrophotometer at  $\lambda_{\max}$  values. The sorbed amount (mg/g) at equilibrium was calculated by the mass balance relationship:

$$q_e = \frac{(C_0 - C_e)V}{W}$$

Where  $C_0$  and  $C_e$  are the initial and equilibrium concentrations (mg/L) respectively.  $V$  is the volume of solution (L),  $W$  is the weight of the sample (g).

Freundlich isotherm model<sup>2,10-2,13</sup> was employed to assess the adsorption equilibrium. The logarithmic form of the Freundlich equation is represented by the following equation:  $\ln q_e = \ln K_f + 1/n \ln C_e$  where  $K_f$  and  $n$  are Freundlich constants related to the adsorption capacity and adsorption intensity, respectively.  $K_f$  and  $1/n$  were obtained from the linear plot of  $\ln q_e$  vs.  $\ln C_e$ . From the intercept and slope of the straight line, the values of  $K_f$  and  $n$  were evaluated.

### 2.3.10 Desorption and reusability study

After completion of first adsorption cycle, azo-dye loaded adsorbents were recovered and kept in aqueous medium on adjusting the pH of the aqueous medium toward very basic region ( $\text{pH} \geq 12$ ) using NaOH. The mixtures were shaken at  $25^\circ\text{C}$  for a period of 24h to desorb azo dyes (MO/OII/OG). Then adsorbents were separated and analyzed for dye concentration in desorbent water using UV-vis spectrophotometer. Desorption amount was calculated using the following equation.

$$\text{Desorption (\%)} = \frac{(C_{\text{des}} \times V_{\text{des}})}{(C_0 - C_e) V_{\text{ads}}} \times 100$$

Where  $V_{\text{des}}$  = volume of desorbent used,

$C_{\text{des}}$  = final concentration of azo dye in solution after desorption

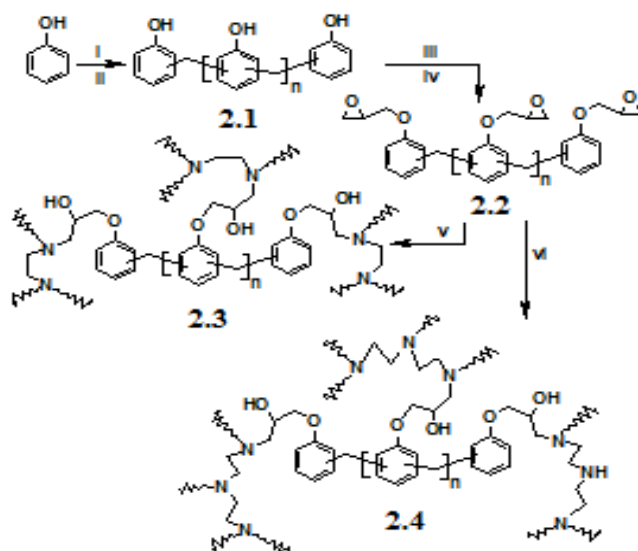
$C_0$  and  $C_e$  are the initial and equilibrium concentrations (mg/L) respectively.

Thereafter, the regeneration process of adsorbents was performed by putting in water with pH adjustment to neutral with dilute HCl / NaOH solution. The resulting regenerated sorbents were filtered, dried and reused in the next cycle. The adsorption capacity of the regenerated network sorbents (2<sup>nd</sup>, 3<sup>rd</sup> and 4<sup>th</sup> runs) was tested under similar conditions.

## 2.4 Results and discussion

### 2.4.1 Synthesis and characterization of novolac-based networks

The route followed for the synthesis of polymeric networks **2.3** and **2.4** is shown in Scheme 2.1. Crosslinkable novolac-based epoxy resin **2.2** is very attractive and extremely useful economic precursor for the preparation of unique polymeric network structures. This was obtained by the glycidylation of novolac. Epoxidation of novolac with an excess of epichlorohydrin eliminates the reaction of phenol hydroxyl groups with glycidylated phenol groups and produces novolac epoxy resin precursor **2.2**.



**Scheme 2.1.** (i) Aqueous formaldehyde (37%), oxalic acid, Reflux, 30 min (ii) Oxalic acid, Reflux, 1h (iii) 1-Chloro-2,3-epoxypropane, NaOH, heat (iv) NaOH, heat (v) Ethylenediamine, 1,4-dioxan/methanol, heat (vi) Diethylenetriamine, dioxin/methanol, heat

It is worthy to note novolac epoxy resin has a strong electron-withdrawing effect that makes the oxirane group highly reactive towards low molecular weight amines, such as ethylenediamine and diethylenetriamine nucleophilic compounds.

The reaction of an epoxy group with primary amine, for instance, ethylene diamine proceeds to yield initially a secondary alcohol and a secondary amine. The secondary amine in turn reacts with epoxy group to produce finally a tertiary amine and two secondary hydroxyl groups leading to polymeric network **2.3** (Figure 2.2). The same crosslinking mechanism with diethylene triamine was proposed to synthesize novolac-based network **2.4**.

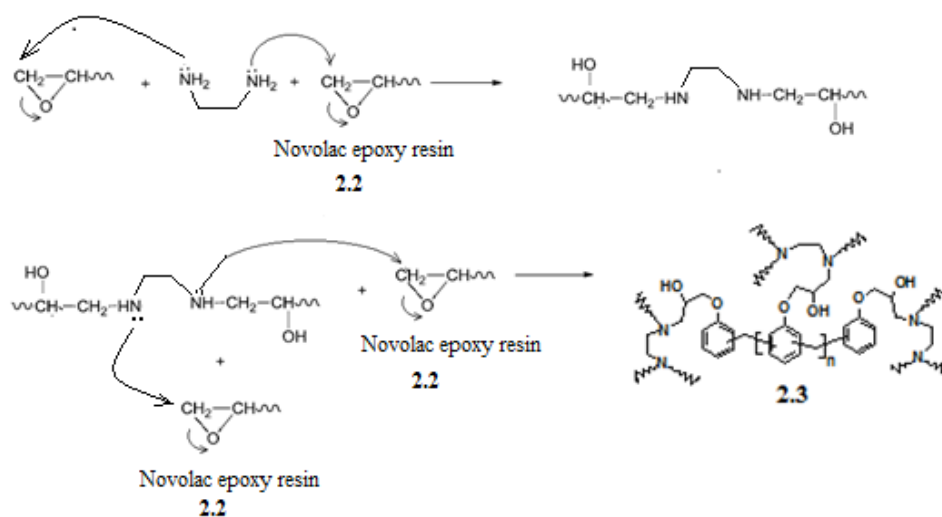


**Figure 2.2.** Reaction mechanism of crosslinking of novolac epoxy resin with ethylenediamine.

Titled macromolecules **2.1** and **2.2** were unequivocally characterized by FTIR and  $^1\text{H}$  NMR analyses. The epoxy resin precursor **2.2** was further characterized by  $^{13}\text{C}$  NMR and GPC analyses. The presence of band at  $904\text{ cm}^{-1}$  indicates the existence of the epoxy functionality. The  $^1\text{H}$ -NMR spectrum of **2.1** (Figure 2.3) exhibits diagnostic peaks in the region  $\delta$  7.16 – 6.66 ppm due to the aromatic protons of the phenol unit and the resonance at  $\delta$  9.31 – 9.11 ppm is indicative of phenolic –OH protons. The introduction of epoxy groups resulted in disappearance of the  $^1\text{H}$  NMR resonances for the protons of phenolic –OH groups. This was further confirmed by the appearance of the signals of epoxy group at  $\delta$  3.98 – 2.83 ppm in the  $^1\text{H}$  NMR spectrum of **2.2** (Figure 2.4). The  $^{13}\text{C}$  NMR spectrum (Figure 2.5) of **2.2** was in full agreement with the proposed structure.

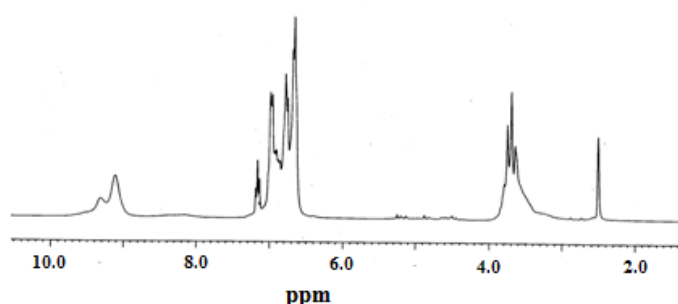


**Figure 2.3**  $^1\text{H}$  NMR spectrum of **2.1**

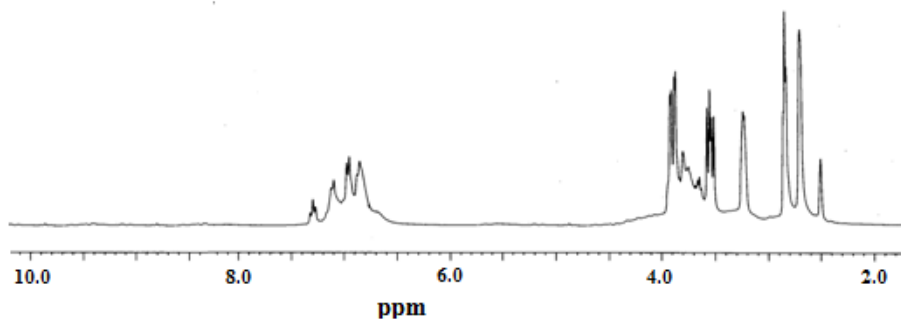


**Figure 2.4** <sup>1</sup>H NMR spectrum of **2.2**

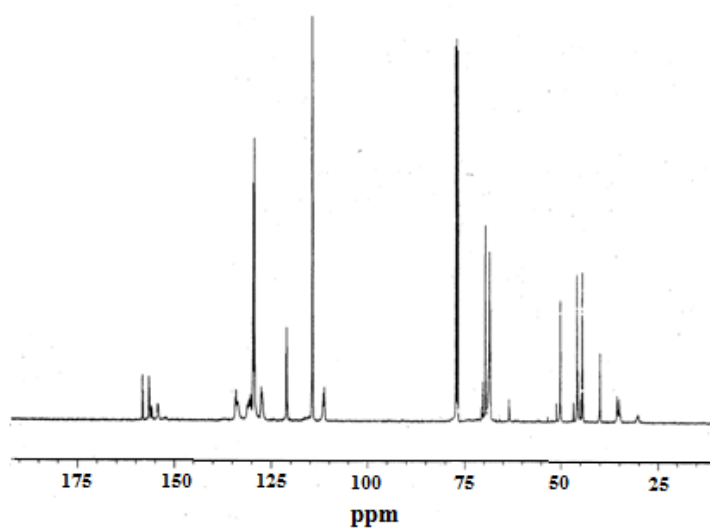


**Figure 2.5** <sup>13</sup>C NMR spectrum of **2.2**

Just like **2.1** and **2.2**, **2.3** and **2.4** could not be dissolved in water and in common organic solvents, so networks have been successfully characterized by FTIR, <sup>13</sup>C NMR, scanning electron microscopy (SEM), BET, thermal

(TGA) and elemental analyses. FTIR spectra of **2.3** and **2.4** (Figure 2.6) reveal the appearance of no peak connected to the C-O stretching vibration in the oxirane or epoxy rings ( $\sim 904\text{ cm}^{-1}$ ). This might be an indication of the participation of ethylenediamine / diethylenetriamine in the epoxide ring opening reaction as depicted in Figure 2.2. In the FTIR spectra of **2.3** and **2.4** (Figure 2.6) the broad absorption bands in the region  $3000 - 3500\text{ cm}^{-1}$  were assigned to O-H and N-H stretching frequencies. The breadth and position of the absorption demonstrate it may be due to a distribution of amino and hydroxyl groups with differing hydrogen bonded geometries in the network structures. The bands occurring at  $1507$  and  $1510\text{ cm}^{-1}$  are associated with N-H plane bending vibrations of **2.3** and **2.4**, respectively. Other characteristic bands that secure assignments to vibrational modes are collected in experimental section.

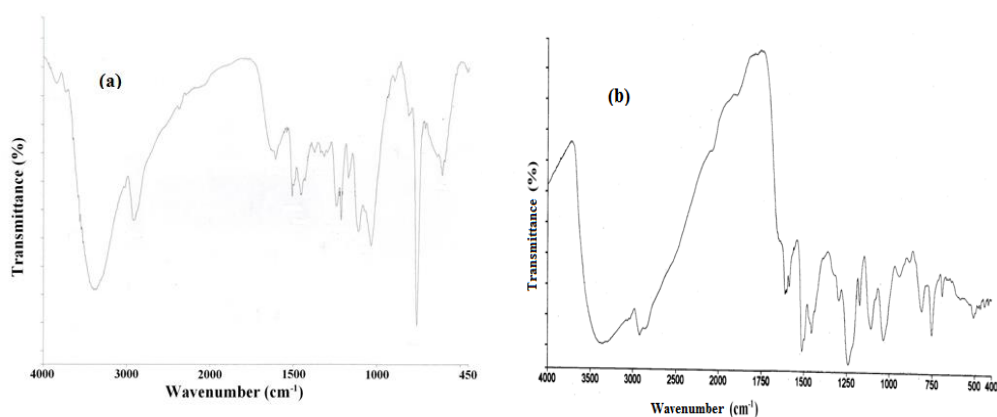


**Figure 2.6** FTIR spectra of (a) **2.3** (b) **2.4**



The assignment of the structures of **2.3** and **2.4** was further supported by the solid state  $^{13}\text{C}$  NMR spectra (Figure 2.7) showing both aromatic and aliphatic carbon signals as listed in the experimental section. The appearance of broad resonance signals in the region 162 – 115 ppm corresponding to the aromatic carbons clearly indicates the existence of novolac skeleton. The signals of saturated carbons related to aliphatic residues of networks were evident at 67 – 39 ppm. Both FTIR and  $^{13}\text{C}$  NMR spectral analyses proved that titled networks were formed by the reaction between ethylenediamine / diethylenetriamine and novolac epoxy resin.

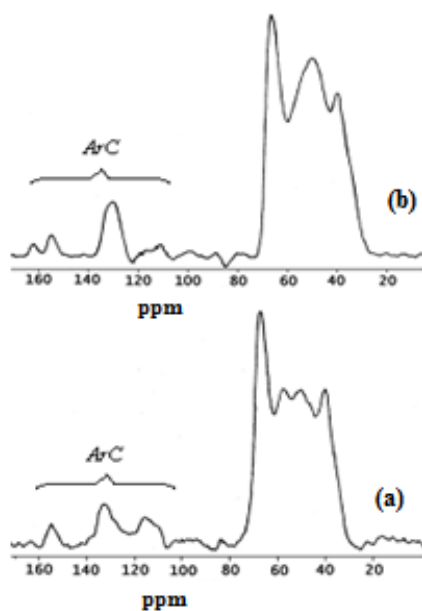


**Figure 2.7** solid state  $^{13}\text{C}$  NMR spectra of (a) **2.3** and (b) **2.4**

Elemental analysis data of the obtained networks unequivocally show the weight percent nitrogen content ensuring the content of amines. The microstructures of networks were studied by SEM. The obtained images (Figures 2.8 and 2.9) at two different magnifications are very close in appearance showing the evidence of porous surface morphology with well-developed pores. It was expected that the micropores would be responsible for the entrapment of azo dye molecules.

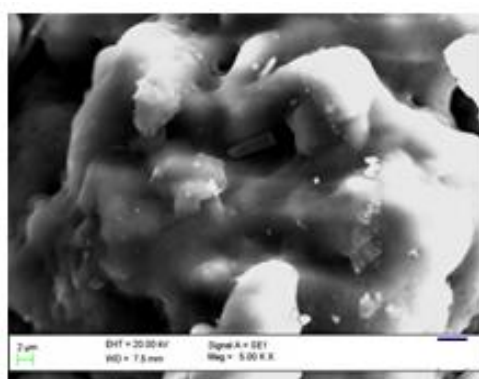


**Figure 2.8** Scanning electron micrograph of 2.3

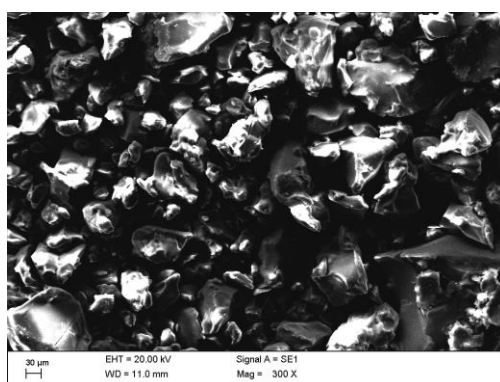


**Figure 2.9** Scanning electron micrograph of 2.4

Thermal properties of **2.3** and **2.4** were examined by TG/DTG (Figure 2.10). The results are summarized in Table 2.1. Thermal degradation beginning at ~267 and ~245 °C with 5-8% weight loss in nitrogen for networks **2.3** and **2.4**, respectively, was observed. All showed a two-step weight loss. However, onset temperature of decomposition of **2.4** is lower than that of **2.3**.

**Table 2.1:** Thermal properties (TG/DTG) of **2.3** and **2.4**.

Network Polymers	TG/DTG*					
	T <sub>d</sub> <sup>5-8</sup> (°C)	Stage	Temp. range (°C)	T <sub>max</sub> (°C)	Weight loss %	Y <sub>c</sub> at 600°C (wt%)
<b>2.3</b>	267	1	267-369	338	47.69	21
		2	369-455	406	43.51	
<b>2.4</b>	245	1	245-384	346	43.59	11
		2	384-482	420	40.61	

\*TGA analysis was performed at a heating rate of 10°C/min under nitrogen flow (100 ml/min); T<sub>d</sub><sup>5-8</sup>= Temperature at which 5-8 % weight loss occurred; T<sub>max</sub>= maximum rate of weight loss; Y<sub>c</sub> = char yield.

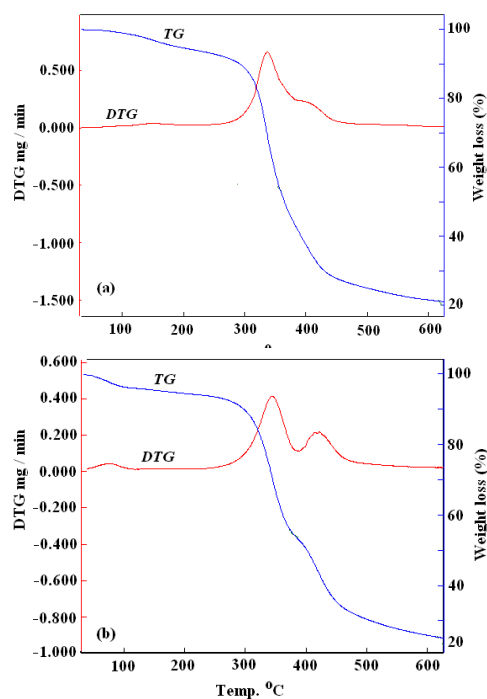


**Figure 2.10** Traces of thermogravimetric analysis (TGA / DTG) of (a) network polymer **2.3** and (b) network polymer **2.4** ( Heating rate of 10°C/min under nitrogen flow (100 ml/min)).

We investigated the swelling behavior of **2.3** and **2.4** in water. As can be seen from this study, the swelling ratio dramatically increased at the initial stage of the contact period of 10 hours, and thereafter reached equilibrium within 48 hours (Figure 2.11).

The high affinity towards the aqueous medium observed is a manifestation of hydrophilic networks. This was anticipated to interact in a similar manner with hydrophilic groups of azo dye molecules.

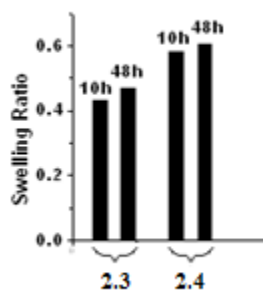


**Figure 2.11** Swelling studies of polymer networks **2.3** and **2.4**.

However, cross-linking density and the number average molecular weight between cross-links in the networks are two important parameters that have reasonable effect on the swelling behavior of polymer networks. These parameters were estimated from the equilibrium swelling data using Flory-Rehner equation<sup>4</sup>.

As shown in Table 2.2, the network **2.4** was found to swell to a greater extent than network **2.3**. This difference in swelling appears to be attributed to a combination of the chemical structure of cross-linking agents, cross-linking density and the number average molecular weight between cross-links in the networks. In addition, the existence of porosity measured by equilibrium swelling study (Table 2.2) is in accordance with what is observed from SEM image. Moreover, the network **2.4** with higher porosity in comparison with **2.3** might be a reflection of the effect of the cross-linking agents and cross-linking density.

As expected, influence of particle sizes on adsorption behaviour is evident. This behaviour could be related to the accessibility of adsorbate surface to the pores of adsorbents. In this context, smaller particles yield larger surface areas exposed to adsorption of adsorbate. Thus, prior to dye adsorption studies, we measured the particle sizes of the sorbent networks. As shown in Figure 2.12, the network powders **2.3** and **2.4** existed in 17 – 219  $\mu\text{m}$  and 18 – 350  $\mu\text{m}$ , respectively, with monomodal size distributions.

**Table 2.2:** Network parameters of **2.3** and **2.4**.

Polymer network	Crosslink density (q)	Number average molecular weight between crosslinks ( $M_c$ )	Porosity (%)
<b>2.3</b>	0.050	9.83	45.27
<b>2.4</b>	0.035	14.20	61.20

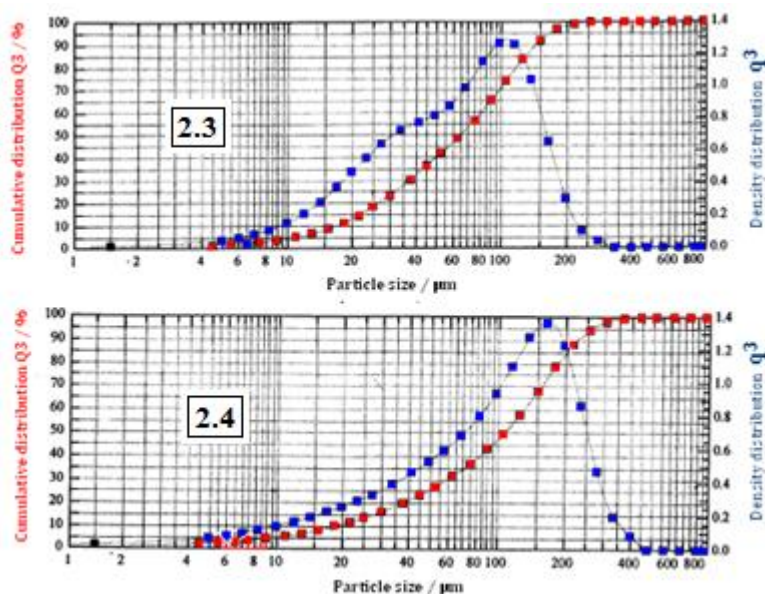


**Figure 2.12.** Size distributions of the network powders **2.3** and **2.4**

The surface area of the formed networks was determined using standard nitrogen adsorption porosimetric technique employing Brunauer-Emmette-Teller ( BET ) method. Table 2.3 summarizes the BET parameters of networks. Network **2.4** showed higher specific surface area and total pore volume than **2.3**, which might result from the fact in structural parameters such as cross-linking agents, cross-linking density and porosity.

**Table 2.3:** BET parameters of **2.3** and **2.4**.

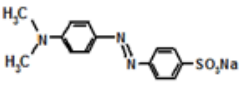
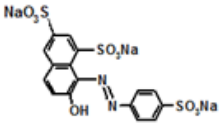
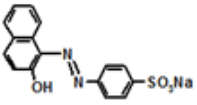
Polymer network	Specific surface area (m <sup>2</sup> /g)	Total pore volume (cm <sup>3</sup> /g)
<b>2.3</b>	7.3555 ± 0.1571	1.689677
<b>2.4</b>	8.9309 ± 0.3158	2.051569

#### **2.4.2 Azo dye adsorption studies**

The popular azo dyes like methyl orange (MO), orange-G (OG) and orange-II (OII) whose characteristics and chemical structures are illustrated in Table 2.4 were used as representative dyes in the evaluation of adsorption abilities of formed network adsorbents. Azo dye adsorption experiments were performed as a function of contact time with initial pH values of 2.30, 7.20 and 10.96. The actual dye containing wastewater has a wide range of initial pH values, and hence the pH is a noteworthy parameter in this study. It suggests

manipulation of the surface charge of adsorbents via protonation-deprotonation of functional groups on variation of pH of the medium, which in turn affects adsorption<sup>2,7,2.8</sup>.

**Table 2.4.** Characteristics of azo dye adsorbates used in adsorption study

Azo dye	Molecular Structure	Colour Index Name
Methyl orange (OG)		Molecular Formula: C <sub>14</sub> H <sub>14</sub> N <sub>3</sub> NaO <sub>3</sub> S Molecular weight (g/mol): 327.33 IUPAC name: Sodium 4-[[4-(dimethylamino)phenyl]diazenyl]benzene-1-sulfonate. Appearance: Orange solid Ionization constant, pK <sub>a</sub> = 3.46 <sup>5</sup> $\lambda_{\max}$ : 460.0 to 470.0 nm(pH 4.8 buffer sol.)
Orange G (OG)		Molecular Formula: C <sub>16</sub> H <sub>10</sub> N <sub>2</sub> Na <sub>2</sub> O <sub>7</sub> S <sub>2</sub> Molecular weight (g/mol): 452.38 IUPAC name: Disodium;7-hydroxy-8-phenyldiazenylnaphthalene-1,3-disulfonate Appearance: Orange solid Ionization constant, pK <sub>a</sub> = 12.8 <sup>6</sup> $\lambda_{\max}$ (water): 475.0 nm
Orange II (OII)		Molecular Formula: C <sub>16</sub> H <sub>11</sub> N <sub>2</sub> NaO <sub>4</sub> S Molecular weight (g/mol): 350.32 IUPAC name: sodium;4-[(2-hydroxynaphthalen-1-yl)diazenyl]benzenesulfonate Appearance: Orange-brown solid Ionization constant, pK <sub>a</sub> = 8.26, 11.4 <sup>6</sup> $\lambda_{\max}$ (water): 484 nm



In the other side, the representative azo dye molecules have different  $pK_a$  values and thus the pH of the medium has marked influence on the degree of ionization of azo-dye adsorbates. Therefore, the pH effect on azo dye adsorption was examined from acidic to basic regions. The pH value was adjusted with dilute NaOH or HCl solutions. The residual concentrations of azo dye solutions fixed at pH values of 2.30, 7.30 and 10.96 were determined using UV/Vis Spectroscopic measurements. Figure 2.13, for instance, shows the gradual decrease in intensity of absorption of azo dye solutions (MO, OG, OII) at different time intervals for network sorbent **2.4**.

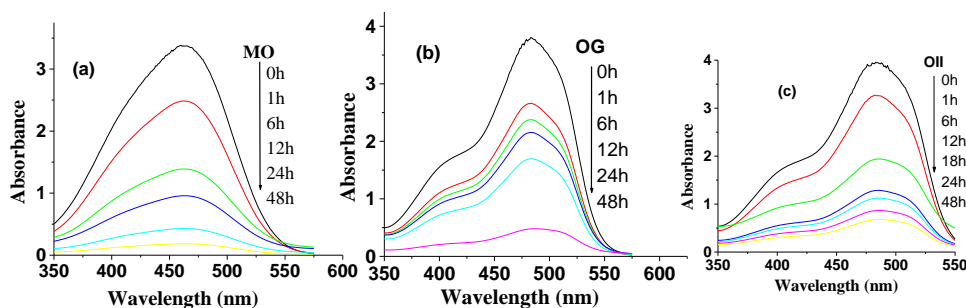


**Figure 2.13.** UV-vis spectral changes of the solutions of (a) MO (  $7.64 \times 10^{-5}M$  ), (b) OG (  $2.21 \times 10^{-4}M$  ) and (c) OII (  $3.06 \times 10^{-4}M$  ) as a function of adsorption time for **2.4**; (pH 7.20, different time intervals, 25°C).

In the pH range from 2.30 to 7.20 (acidic to neutral condition), the dye uptake capacities of network adsorbents at the initial phase of contact time were very rapid attaining adsorption equilibrium within 48 h. Figures 2.14 and 2.15, for instance, show the adsorption of MO and OII onto **2.4** reached the equilibrium

in 48h. The rapid adsorption at the initial stage of contact was probably due to the abundant availability of the porosity surface of the adsorbents. Thereafter the dye uptake rate was found to be slow reflecting probably the slow pore diffusion of the dyes into the bulk of the sorbent networks. The fast adsorption rate at the initial stage has practical advantages in terms of reducing reactor volumes and times. Compared with MO, the more effective adsorption of OII and OG onto sorbent networks was observed at this pH range indicating more favorable interaction.

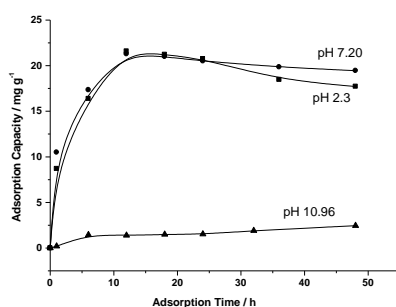


**Figure 2.14.** The effect of adsorption time on MO adsorption capacity of 2.4

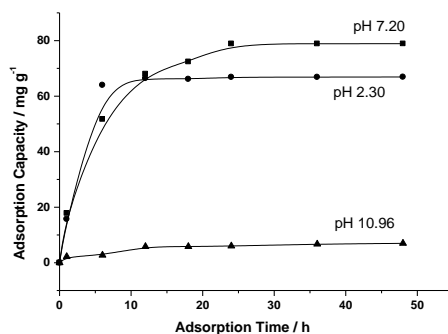


**Figure 2.15.** The effect of adsorption time on OII adsorption capacity of 2.4

Meanwhile, the adsorbents showed very low or almost no dye adsorption at pH 10.96 (basic condition). Moreover, the dye uptake capacity of **2.4** was found to be higher than that of **2.3** under similar conditions as evidenced from Figures 2.16, 2.17 and 2.18 demonstrating the impact of diethylenetriamine unit on adsorption of such anionic dyes.

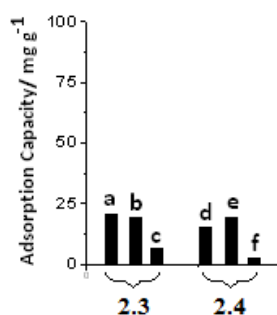


**Figure 2.16.** Effect of pH on the azo dye adsorption capacity of **2.3** and **2.4** (a, d: pH = 2.30; b, e: pH = 7.20; c, f: pH = 10.96; t = 48h; T= 298 K); MO adsorption ( $C_0 = 7.64 \times 10^{-5}M$ ).

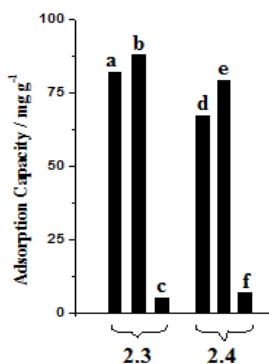


**Figure 2.17.** Effect of pH on the azo dye adsorption capacity of **2.3** and **2.4** (a, d: pH = 2.30; b, e: pH = 7.20; c, f: pH = 10.96; t = 48h; T= 298 K); OII adsorption ( $C_0 = 3.06 \times 10^{-4}M$ ).

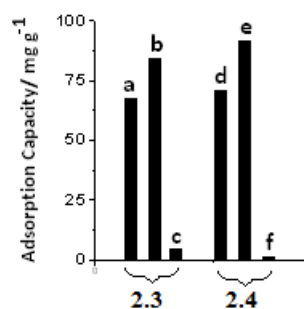


**Figure 2.18.** Effect of pH on the azo dye adsorption capacity of **2.3** and **2.4** (a, d: pH = 2.30; b, e: pH = 7.20; c, f: pH = 10.96; t = 48h; T= 298 K); OG adsorption ( $C_0 = 2.21 \times 10^{-4}M$ ).

The adsorption isotherm indicates the fractional distribution of azo-dye adsorbate within the solid (adsorbent) and liquid (solution) phases when the adsorption process is at equilibrium at a constant temperature and pH<sup>2.9</sup>. The equilibrium adsorption isotherm data collected at initial pH values of 2.30 and 7.20 were fitted with Freundlich model<sup>2.10-2.13</sup>. The model parameters ( $n$ ,  $K_f$ ) along with the correlation coefficients ( $R^2$ ) were obtained from the graphical plots of  $\ln q_e$  against  $\ln C_e$  as presented in Figures 2.19 – 2.24.

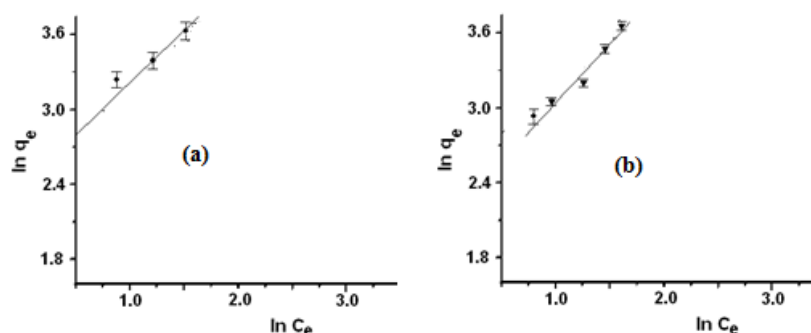


**Figure 2.19.** Freundlich isotherms for the adsorption of MO onto **2.3** at (a) pH 2.30 (-●-) and (b) pH 7.20 (-▼-) at 25°C

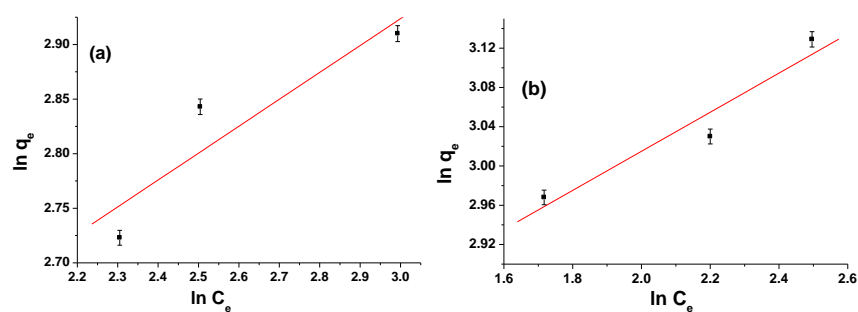


**Figure 2.20.** Freundlich isotherms for the adsorption of MO onto **2.4** at (a) pH 2.30 and (b) pH 7.0 at 25°C

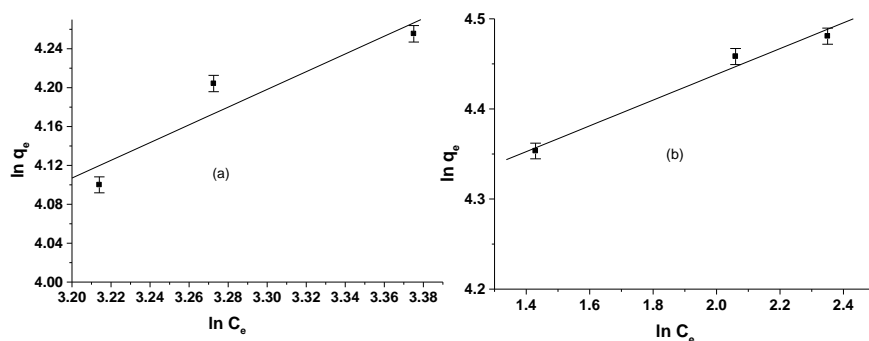


**Figure 2.21.** Freundlich isotherms for the adsorption of OII onto **2.3** at (a) pH 2.30 and (b) pH 7.20 at 25°C

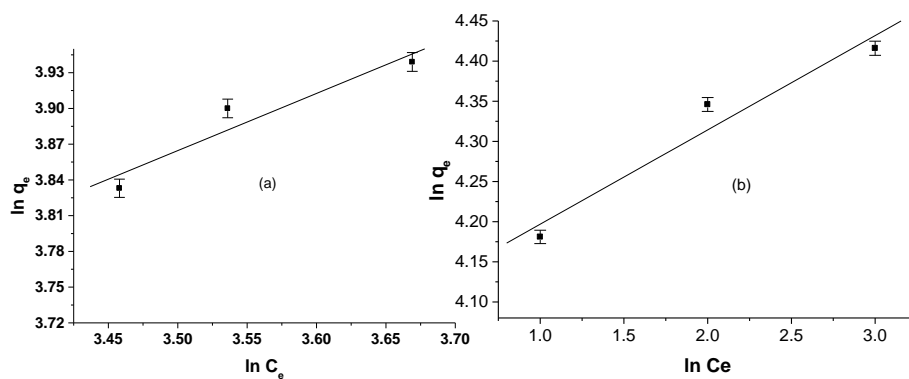


**Figure 2.22.** Freundlich isotherms for the adsorption of OII onto **2.4** at (a) pH 2.30 and (b) pH 7.20 at 25°C

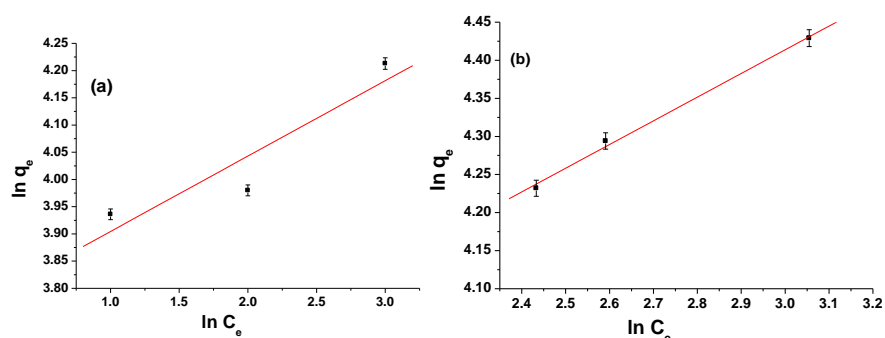


**Figure 2.23.** Freundlich isotherms for the adsorption of OG onto **2.3** at (a) pH 2.30 and (b) pH 7.0 at 25°C

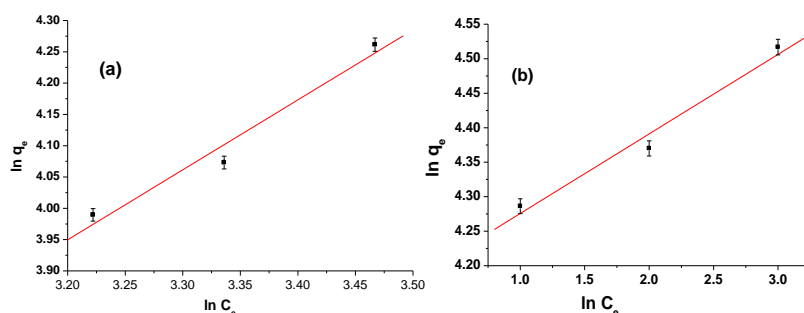


**Figure 2.24.** Freundlich isotherms for the adsorption of OG onto **2.4** at (a) pH 2.30 and (b) pH 7.0 at 25°C

The values of isotherm model parameters along with the correlation coefficients ( $R^2$ ) obtained from these plots (Figures 2.19 – 2.24) were listed in Table 2.5. The  $K_f$  values indicate the good adsorption capacity of network adsorbents. The values of  $n$  at pH = 2.30 – 7.0 demonstrate thermodynamically favorable adsorption characteristics ( $10 > n > 1$ )<sup>2,14-2,16</sup>. The values of regression coefficients ( $R^2$ ) between 0.87 and 0.9978 reflected the fair fitting of Freundlich isotherm model to the experimental data. Therefore,

pH value of the solution was an important parameter in the manipulation of azo dye adsorption capacities of adsorbent materials.

**Table 2.5:** Freundlich Constants of the adsorption isotherms for representative azodyes (MO, OII and OG) onto **2.3** and **2.4** at different pH values at 25°C.

Polymer network	Azodye	pH	Freundlich Constants		
			$K_f$	n	$R^2$
<b>2.3</b>	MO	2.30	10.699	1.193	0.8771
		7.20	8.111	1.057	0.9445
	OII	2.30	3.212	1.096	0.8819
		7.20	63.596	6.997	0.9788
	OG	2.30	43.206	7.220	0.9304
		7.20	32.496	3.216	0.9978
<b>2.4</b>	MO	2.30	8.886	4.05	0.9207
		7.20	13.678	4.97	0.9610
	OII	2.30	8.887	2.083	0.9123
		7.20	59.105	8.510	0.9483
	OG	2.30	3.058	2.686	0.9681
		7.20	64.097	8.673	0.9757

To get further insight into the qualitative information on the chemical interactions FTIR spectra of isolated dye-adsorbed networks (dry) were recorded. The chemical interactions between networks and representative azo dyes have been confirmed in our published reports<sup>2.1-2.3</sup>. The broad absorption band in the region 3000 – 3500  $\text{cm}^{-1}$  corresponded to O-H and N-H stretching frequencies become better resolved in the dye-adsorbed networks. Meanwhile, the peaks at 1173 and 1034  $\text{cm}^{-1}$  of the dye-loaded networks were assigned to the asymmetric and symmetric stretching vibrations of azo dye  $\text{SO}_3^-$  groups. These assigned peaks are at lower wavenumber ( $\Delta\nu = 6\text{-}15 \text{ cm}^{-1}$ ) than in the pure azo dye molecules. The shifting of these peaks provides solid evidence

that adsorbed azo dye molecules involve chemical interaction with the designed polymer networks.

In accordance with our reports<sup>2.1-2.3</sup>, the pH dependent adsorption of azo dyes onto prepared adsorbents may be ascribed to the ionic interaction as well as hydrogen bonding interactions. Figure 2.25 outlines the anticipated mechanism of the pH-dependent adsorption.

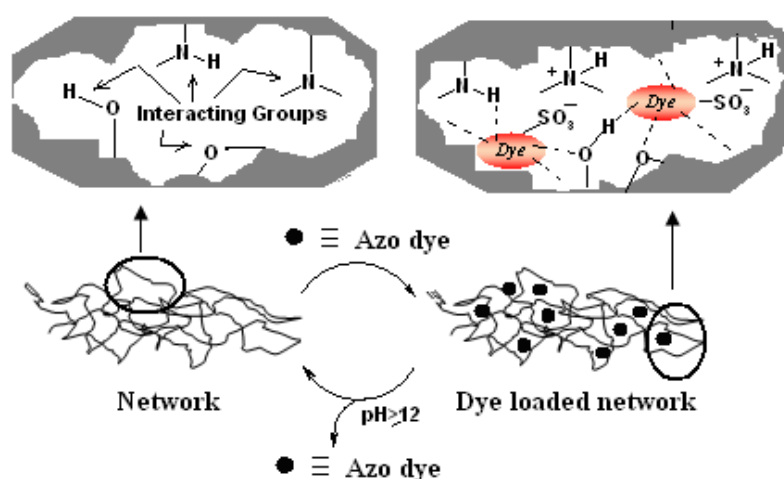


**Figure 2.25** A proposed mechanism of adsorption: chemical interactions occurring within the network adsorbents

Varying number of interacting groups (amino, hydroxy and ether functionalities) into the domains of networks played important role to favour binding of hydrophilic azo dyes. In the acidic ( $\text{pH} = 2.30$ ) to nearly neutral region ( $\text{pH} = 7.20$ ) strong electrostatic interaction established between the protonated amino groups ( $-\text{N}^+$ ) and sulphonate groups ( $-\text{SO}_3^-$ ) as well as



hydrogen bonding interactions ( $^+N-H\cdots^-O_3S-$  and  $-O-H\cdots^-O_3S-$ ) are the main driving forces behind the adsorption of azo dyes. However, it is seen that the adsorbents achieved stronger uptake of OII and OG than MO under these pHs attributing to the presence of more number of functional groups in the structures of OII and OG. Significant drop in adsorption capacity of the network adsorbents in the experiments performed in the basic medium ( pH = 10.96 ) can be attributed to only weak hydrogen bonding forces. In addition, the hydroxyl ion ( $OH^-$ ) may compete with anionic azo dye molecules for sorption sites, which could result in a decline in the removal of dyes. Previous reports on the pH-dependent known behaviours of structurally related molecules<sup>2,17,2.18</sup> support the protonation / ionization of amino and sulphonate groups.

Presence of inorganic salts, in particular NaCl, promotes enhancement of dye molecules out of solution onto fibers during dyeing process<sup>2.19</sup>. Thus, NaCl is often present in dye-containing wastewaters. Therefore, knowledge on the effect of NaCl as one of the salting-out agents is necessary for a proper assessment of the efficiency of adsorbents in removing dye molecules. In this context, adsorption equilibrium was further investigated in presence of NaCl, while keeping the other parameters constant. It is noteworthy to mention that the addition of sodium chloride (0.1 M) hardly affected the equilibrium adsorption of azo dye molecules. This observation suggests that strong interactions (ionic and hydrogen bonding) established between sorbent

network and dye molecules are essentially independent of salting-out effect, which is significant from practical point of view.

It was also observed that the yellow colored sorbents became red with concomitant decolorization of dye solutions after the adsorption process. Figure 2.26, for instance, shows distinct color change of network sorbent on adsorption of MO. This is a visual indication of the adsorptive coverage of sorbent surface with dye molecules.



**Figure 2.26** Azo dye (MO) adsorption for 48h onto network polymer matrix associated with visual color change

### **2.4.3 Desorption and reusability study**

Assessment on the reusability of adsorbents and dye recovery is very important for practical applications. Further to compute reusability, desorption from the dye-loaded sorbents was made on adjusting the pH of the aqueous medium toward very basic region ( $\text{pH} \geq 12$ ). The maximum desorption of dye molecules adsorbed was almost 90% indicating the reusability of sorbents. The regeneration efficiency was found to retain above 80% after the third cycle. Such reusability and regeneration potential of the sorbent networks reflects the economic success of the adsorption process.

#### **2.4.4 Importance of the work**

Because of the simplicity in synthesis, pH-induced adsorption of azo dye molecules and pH-driven regeneration, the sorbent networks should have potential application in remediation technology and environmental sciences aiming to the treatment of azo dye-containing effluents and analytical chemistry. Their azo dye adsorption capacities are comparable to other adsorbents reported in literatures. Moreover, the increasing cost of conventional adsorbents undoubtedly makes novolac-based materials of adjustable surface chemistry to be the most attractive adsorbents for wastewater treatment.

#### **2.5 Conclusion**

This chapter gives a full account of the syntheses, characterization and azo dye adsorption properties of network polymers **2.3** and **2.4** derived from low cost crosslinkable novolac-based epoxy resin. The structural and physicochemical properties of obtained networks were studied using FTIR, <sup>13</sup>C NMR, SEM, BET, thermal (TGA) and elemental analyses. The synthesised networks revealed consistent potential for adsorption of typical azo dyes like MO, OII and OG. The highest uptake of OG by sorbent networks might be ascribed to

the presence of more number of attractive functional groups ( two sulphonate groups and hydroxyl group ) compared with OII and MO. The adsorption process was found to be dependent on pH, an important parameter optimizing surface charges of network structures for the adsorption of charged adsorbates. Adsorption of selected azo dyes under study was favored at pH 2.30 and 7.20. Equilibrium adsorption data obtained were fitted to Freundlich isotherm model. The result indicates that adsorption is a typical physical process (  $n > 1$  ). FTIR studies provide information about the molecular sites which are involved in the dye binding process. pH-driven adsorption-desorption cycle shows that networks are good reusable adsorbing materials for azo dye pollutants. Moreover, facile regeneration of used sorbents also recovers the azo dyes so they can be disposed of properly or purified for reuse. Publications were achieved from the accomplishment of this research.

## **2.6 Further scope of work**

The author recommends the further research:

- i) Although the developments of novolac-based network materials are extremely interesting, further research to investigate the adsorption capacities of such materials toward a variety of azo dye colorants is required.

- ii) The synthesized networks are particularly appealing in the design of polymer/inorganic hybrid materials for the removal of diverse azo dye pollutants from waters.
- iii) Crosslinkable novolac epoxy resin as synthesized offers opportunities to develop varieties of novolac-based network materials by incorporating various amines including natural polymers like chitosan. This can be potential functional approach to manipulate the adsorption sites for the efficient removal of targeting azo dye pollutants.
- iv) Excavation of the full potential of network sorbents for removing azo dye colorants from real industry wastewater samples will also demand further studies.